Nature of quantum spin liquids of the $S = \frac{1}{2}$ Heisenberg antiferromagnet on the triangular lattice: A parallel DMRG study

Yi-Fan Jiang [1,2] and Hong-Chen Jiang[2,*]

[1]*School of Physical Science and Technology, ShanghaiTech University, Shanghai 201210, China*
[2]*Stanford Institute for Materials and Energy Sciences, SLAC National Accelerator Laboratory and Stanford University,*
Menlo Park, California 94025, USA

We study the ground-state properties of the quantum spin liquid (QSL) phases of the spin-1/2 antiferromagnetic Heisenberg model on the triangular lattice with nearest- (J_1), next-nearest- (J_2), and third-neighbor (J_3) interactions by using the density-matrix renormalization group (DMRG) method. By combining parallel DMRG with SU(2) spin rotational symmetry, we are able to obtain accurate results on large cylinders with length up to $L_x = 48$ and circumference $L_y = 6–12$. Our results suggest that the QSL phase of the J_1-J_2 Heisenberg model is gapped, which is characterized by the absence of a gapless mode and by short-range spin-spin and dimer-dimer correlations. In the presence of J_3 interaction, we find that a critical QSL with a single gapless mode emerges. While both spin-spin and scalar chiral-chiral correlations are short ranged, dimer-dimer correlations are quasi long ranged and decay as a power law at long distances.

Introduction. Quantum spin liquids (QSLs) are highly entangled phases of matter that exhibit novel features associated with their topological character and support fractional excitations, yet resist symmetry breaking even down to zero temperature due to strong quantum fluctuations and geometric frustrations [1–3]. Broad interest in QSLs was triggered by their important role in understanding strongly correlated materials, especially high-temperature superconductors, as well as their potential application in topological quantum computation [3–8]. One of the most promising systems to realize QSLs is the spin-1/2 Heisenberg antiferromagnet on the triangular lattice, which is defined by the model Hamiltonian

$$H = \sum_{ij} J_{ij} \mathbf{S}_i \cdot \mathbf{S}_j. \tag{1}$$

A number of studies of the J_1-J_2 model with first- (J_1) and second-neighbor (J_2) exchange couplings have led to a consensus that there is an intermediate QSL phase (referred to as a J_1-J_2 spin liquid) in the range $0.07 < J_2/J_1 < 0.15$, which is sandwiched by the 120° magnetic phase and a stripe magnetic phase [9–28]. However, its precise nature remains still under intense debate; distinct types of QSLs have been proposed including the gapped spin liquid [13–18], the gapless U(1) Dirac spin liquid [19,20], and the spin liquid with spinon Fermi surface [28]. The gapped spin liquid is characterized by a fully gapped excitation spectrum, and all the correlations, including the spin-spin, dimer-dimer, and scalar chiral-chiral correlations, are short ranged. While the spin-spin correlation is quasi long ranged in both the Dirac and spinon Fermi surface spin liquids, the former is gapless only at specific discrete momenta in the reciprocal space, and the latter is gapless on

the whole spinon Fermi surface. As a result, a further unbiased study is required to identify the precise nature of the J_1-J_2 spin liquid phase.

Aside from the J_1 and J_2 interactions, an additional third-neighbor J_3 interaction (referred to as the J_1-J_2-J_3 model) has also been considered in recent studies; it was proposed as an important ingredient to understand various magnetic properties of the triangular lattice materials $CeFeO_2$ and $CuCrO_2$ [29–32]. Interestingly, a recent study [28] has provided numerical evidence that a new type of chiral spin liquid (CSL) state could be realized in the J_1-J_2-J_3 model, which spontaneously breaks the time-reversal symmetry (TRS) and has long-range scalar chiral order. Distinct with the Kalmeyer-Laughlin state [33], this CSL has a spinon Fermi surface with a gapless excitation spectrum. However, the spin-spin correlations decay exponentially, which seems inconsistent with the presence of the spinon Fermi surface. To resolve the discrepancy and understand the QSL phase of the J_1-J_2-J_3 model, further numerical simulation is required.

In this Research Letter, we address the above questions by studying both the J_1-J_2 and J_1-J_2-J_3 models on triangular cylinders with circumference $L_y = 6–12$ and length up to $L_x = 48$ using the density-matrix renormalization group (DMRG) encoded with SU(2) spin rotational symmetry [34–36]. Specifically, we have developed an efficient parallel DMRG scheme and performed both real- and complex-value DMRG simulations. The parallel scheme [36], which is based on equally distributing the Hamiltonian, has further improved the numerical efficiency by $O(L_y)$ times, so that we are able to keep up to $m = 9000$ SU(2) states [equivalent to $m = 36\,000$ U(1) states] in the complex-value DMRG simulation to obtain accurate results.

For more reliable results, we focus on typical sets of parameters deep inside the QSL phases of both models used in previous studies [13–15,19,20,28]. Our results suggest that
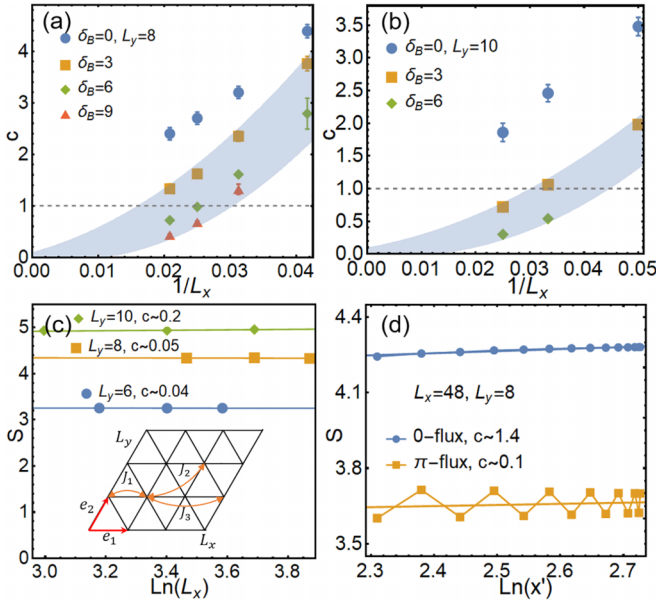
FIG. 1. Entanglement entropy S and central charge c for the J_1-J_2 model. The extracted c with $J_2 = 0.11$ on (a) $L_y = 8$ and (b) $L_y = 10$ cylinders using Eq. (2), where δ_B is the number of data points omitted from the open boundaries. The shaded regions are guides for the eye. (c) $S(L_x/2)$ as a function of $\ln(L_x)$ on $L_y = 6, 8, 10$ cylinders, where solid lines denote the fitting $S(L_x/2) \sim \frac{c}{6} \ln(L_x)$. (d) $S(x)$ on $L_y = 8$ cylinder with length $L_x = 48$ with a 0 or π flux inserted through the cylinder, where $x' = \frac{L_x}{\pi} \sin \frac{\pi x}{L_x}$.

the J_1-J_2 spin liquid is consistent with a gapped QSL [37,38], where all correlations, including the spin-spin, dimer-dimer, and scalar chiral-chiral correlations, are short ranged and decay exponentially at long distances. In the presence of J_3 interaction, we find that a new type of QSL, dubbed a critical spin liquid [39,40], emerges in the J_1-J_2-J_3 model. There is a single gapless mode which is independent of the circumference of the cylinders. While both spin-spin and scalar chiral-chiral correlations are short ranged, the dimer-dimer correlations are quasi long ranged.

Model and method. We employ DMRG [34–36] to study the ground-state properties of the spin-1/2 antiferromagnetic Heisenberg model on the triangular lattice defined in Eq. (1). The lattice geometry used in our simulations is depicted in the inset of Fig. 1(c), with open (periodic) boundary conditions along the e_1 (e_2) direction, where $e_1 = (1, 0)$ and $e_2 = (1/2, \sqrt{3}/2)$ are two basis vectors. We focus on cylinders with circumference L_y and length L_x, where L_y and L_x are the number of sites in the e_2 and e_1 directions, respectively. We set $J_1 = 1$ as an energy unit and focus on two typical sets of parameters used in previous studies [28]. These correspond to the J_1-J_2 model with $J_2 = 0.11$, and the J_1-J_2-J_3 model with $J_2 = 0.3$ and $J_3 = 0.15$, respectively. In this Research Letter, we report results on $L_y = 6$–12 cylinders of length up to $L_x = 48$.

We perform both real- and complex-value DMRG simulations and keep up to $m = 9000$ SU(2) states [equivalent to $m = 36\,000$ U(1) states] in each DMRG block, where the complex-value simulation is employed to directly detect potentially spontaneous time-reversal-symmetry breaking in

the system. To conquer the extensive numerical cost, especially on wide cylinders with a large number of states, we have developed an efficient operator-level parallel DMRG scheme with SU(2) spin rotational symmetry. The operator-level parallelism is realized by dynamically distributing the decomposed Hamiltonian to computing nodes in each step of the DMRG simulation. For both models, most parts of the SU(2) DMRG simulation can be accelerated by $n \sim 2L_y$ times. For the U(1) DMRG simulation, $n \sim 6L_y$. An obvious advantage of the operator-level parallelization over the real-space parallelization [41] is that it does not introduce any additional approximation compared with the single-node DMRG simulation. Meanwhile, parallel DMRG simulation can also be achieved by distributing matrix-vector contraction or blocks with different quantum numbers to the nodes or generalizing the two-site DMRG algorithm to the N-site version [42–45]. Further details of the operator-level parallel DMRG scheme are provided in the Supplemental Material [46].

J_1-J_2 model. The central debate regarding the J_1-J_2 spin liquid is whether it is gapped or gapless. A key diagnostic to distinguish distinct types of QSLs proposed in previous studies is the number of gapless spin modes, i.e., the central charge c. The gapped QSL has no gapless spin mode with $c = 0$ [13–15]. For the U(1) Dirac spin liquid, $c \leqslant 3$, which depends on the momentum cut across the Dirac points [19,20]. In contrast, for the spin liquid with spinon Fermi surface, the value of c increases with the width L_y of the systems [28].

To better identify the nature of the J_1-J_2 spin liquid, we focus on $J_2 = 0.11$, which is deep inside the spin liquid phase of the J_1-J_2 model. We first calculate the von Neumann entanglement entropy $S(x) = -\text{Tr}[\rho_x \ln \rho_x]$ on numerous cylinders where ρ_x is the reduced density matrix of the subsystem with length x. For a critical system of length L_x with open boundaries, it has been established that c can be obtained using [47,48]

$$S(x) = \frac{c}{6} \ln \left[\frac{L_x}{\pi} \sin \frac{\pi x}{L_x} \right] + \text{const}, \qquad (2)$$

where examples are shown in Fig. 1. It should be noted that notable finite-size and boundary effects have been observed associated with Eq. (2), from which c could be dramatically overestimated. To extract c more reliably, we have systematically analyzed both the boundary and finite-size effects. For instance, for a given cylinder of length L_x, we extract c using Eq. (2) with data points $x \in [1 + \delta_B, L_x - \delta_B]$ by removing δ_B data points from both open ends. As shown in Figs. 1(a) and 1(b), the extracted c decreases monotonically and rapidly with the increase in both L_x and δ_B. It is worth mentioning that for a given cylinder of length L_x, the reduced boundary effect brought about by removing several data points from the open ends can provide more reliable results that are much closer to those in the long-cylinder limit. In the long-cylinder limit $L_x \to \infty$, i.e., $1/L_x \to 0$, we find that $c \sim 0$ for $L_y = 6$–10 cylinders. Alternatively, we can reduce the boundary effect by using a modified formula involving only two data points in the middle of the cylinders [49] to extract the central charge, which gives us similar results, as shown in the Supplemental Material [46]. This suggests that the J_1-J_2 spin liquid is gapped without a gapless spin mode.
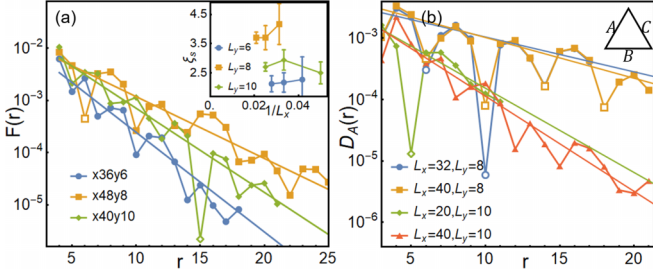
FIG. 2. Spin-spin $F(r)$ and dimer-dimer $D_A(r)$ correlations of the J_1-J_2 model. (a) $F(r)$ with $J_2 = 0.11$ on $L_y = 6, 8, 10$ cylinders, where solid lines denote the exponential fitting $F(r) \sim e^{-r/\xi_s}$ using filled data points. Inset: Correlation length ξ_s on $L_y = 6, 8, 10$ cylinders as a function of $1/L_x$. (b) $D_A(r)$ on $L_y = 8$ and $L_y = 10$ cylinders with length $L_x = 20, 32, 40$, where solid lines denote the exponential fitting $D_A(r) \sim e^{-r/\xi_A}$ using the envelope of the data points (filled symbols). A, B, and C denote the three different bonds.

As a further test, we have also studied the effect of twisted boundary conditions, for instance, antiperiodic boundary conditions, by inserting a π flux through the cylinder, which changes the transverse part of the spin interaction, $S_i^+ S_j^- +$ H.c. $\rightarrow e^{i\theta} S_i^+ S_j^- +$ H.c. with $\theta = \pi$, on the bonds crossing the periodic boundary around the cylinder. This is simulated by the parallel DMRG with U(1) symmetry due to the broken spin SU(2) symmetry. Figure 1(d) shows an example of $S(x)$ on an $L_y = 8$ cylinder of length $L_x = 48$ with periodic (0-flux) and antiperiodic (π-flux) boundary conditions. The extracted central charge with a π flux is $c \sim 0.1$, which is much closer to $c = 0$ than the value found for the normal cylinder is. Alternatively, c can be obtained using $S(L_x/2) = \frac{c}{6} \ln(L_x) + \text{const}$ as shown in Fig. 1(c), which is $c = 0.10(1)$ and $c = 0.09(5)$ for $L_y = 8$ and $L_y = 10$ cylinders, respectively. Similar behavior has also been observed on $L_y = 12$ cylinders (see Supplemental Material [46] for details). All of these are consistent with a gapped state without a gapless spin mode.

The absence of a gapless mode suggests that all correlations are short ranged. To see this, we first calculate the spin-spin correlation function defined as

$$F(r) = \left| \langle \mathbf{S}_{(x_0, y_0)} \cdot \mathbf{S}_{(x_0+r, y_0)} \rangle \right|. \quad (3)$$

Here, $\mathbf{S}_{(x_0, y_0)}$ is the spin operator on the reference point $(x_0, y_0) = (L_x/4, L_y/2)$, and r is the distance between two sites in the $\mathbf{e}_1$ direction. Figure 2(a) shows examples of $F(r)$ for $L_y = 6, 8, 10$ cylinders. For all cases, $F(r)$ decays exponentially at long distances and can be well fitted by an exponential function $F(r) \sim e^{-r/\xi_s}$ with finite correlation length ξ_s shown in the inset of Fig. 2(a). The fact that ξ_s decreases with the increase in L_y when $L_y \geqslant 8$ (see Supplemental Material [46] for details) suggests a finite ξ_s in two dimensions.

We have also measured the dimer-dimer correlation function defined as

$$D_a(r) = \langle (\hat{B}_a(x, y) - \langle \hat{B}_a(x, y) \rangle)$$
$$\times (\hat{B}_a(x + r, y) - \langle \hat{B}_a(x + r, y) \rangle) \rangle. \quad (4)$$

Here, $\hat{B}_a(x, y) = \mathbf{S}(x, y) \cdot \mathbf{S}(x_a, y_a)$ is the dimer operator on bond type $a = A$, B, or C shown in Fig. 2(b). We find that
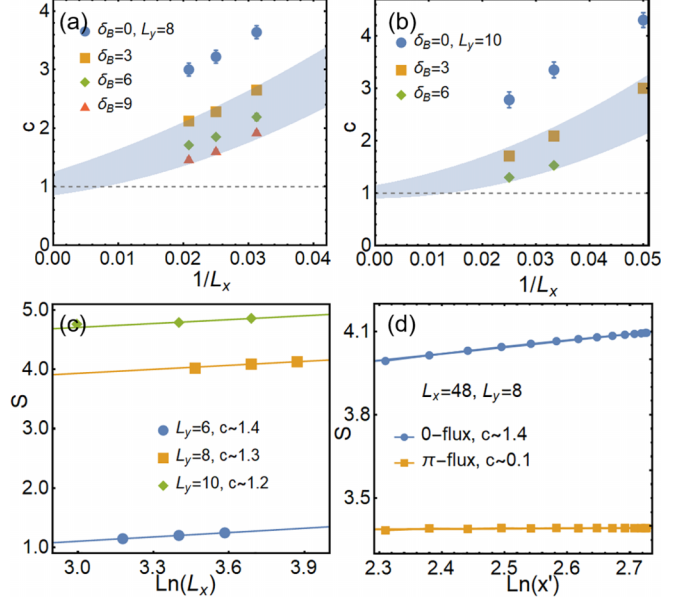

FIG. 3. Entanglement entropy S and central charge c for the J_1-J_2-J_3 model. (a) The extracted c with $J_2 = 0.3$ and $J_3 = 0.15$ on (a) $L_y = 8$ and (b) $L_y = 10$ cylinders, where δ_B is the number of data points omitted from the open boundaries. The shaded regions are guides for the eye. (c) $S(L_x/2)$ as a function of $\ln(L_x)$, where solid lines denote the fitting $S(L_x/2) \sim \frac{c}{6} \ln(L_x)$. (d) $S(x)$ on an $L_y = 8$ cylinder of length $L_x = 48$ with a 0 or π flux inserted through the cylinder. The solid lines denote the fitting $S(x) \sim \frac{c}{6} \ln(x')$, where $x' = \frac{L_x}{\pi} \sin(\frac{\pi x}{L_x})$.

while the strength of $B_a = \langle \hat{B}_a(x, y) \rangle$ depends on a due to the broken C_3 rotational symmetry of the cylindrical geometry, it has no any spatial oscillation in the bulk of the systems, suggesting the absence of static long-range dimer order. This is further evidenced by the fact that $D_a(r)$ decays exponentially as $D_a(r) \sim e^{-r/\xi_a}$ with finite correlation length ξ_a. As shown in Fig. 2(b), the correlation length ξ_A on long cylinders with fixed width L_y does not notably depend on system length L_x. When the cylinder becomes wider, we find a decrease in the correlation length from $\xi_a \sim 6.5$ on $L_y = 8$ cylinders to $\xi_a \sim 2.8$ on $L_y = 10$ cylinders.

J_1-J_2-J_3 *model*. In the presence of J_3 interaction, a recent study [28] suggests that a distinct QSL state, i.e., a gapless CSL with spinon Fermi surface, can be realized in the J_1-J_2-J_3 model. To rule out the possible finite-size effect, we follow the same procedure with the J_1-J_2 model. For simplicity, we focus on the same set of parameters as were used in Ref. [28], i.e., $J_2 = 0.3$ and $J_3 = 0.15$, which is deep inside the QSL phase. We first benchmark our calculations using the same parameters and have observed consistency for both $L_y = 6$ cylinders and an $N = 16 \times 8$ cylinder [28]. (See Supplemental Material [46] for details.) However, similar to the J_1-J_2 model, we find that the extracted c on $L_y = 8$ cylinders suffers from notable finite-size and boundary effects, which decreases monotonically with the increase in L_x as shown in Fig. 3(a). In the long-cylinder limit $L_x \rightarrow \infty$, it approaches a much smaller value, $c \sim 1$, suggesting that there is only one gapless mode on an $L_y = 8$ cylinder. This is also true on $L_y = 10$ cylinders, where we also find $c \sim 1$ as shown in Fig. 3(b). Similar results
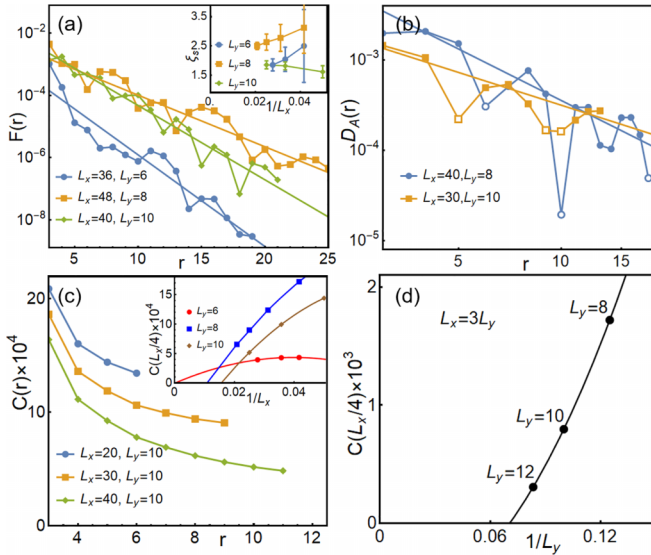
FIG. 4. Correlation functions for the J_1-J_2-J_3 model. (a) Spin-spin correlation $F(r)$ with $J_2 = 0.3$ and $J_3 = 0.15$ on $L_y = 6, 8, 10$ cylinders. Solid lines denote the exponential fitting $F(r) \sim e^{-r/\xi_s}$. Inset: correlation length ξ_s as a function of $1/L_x$. (b) Dimer-dimer correlation $D_A(r)$ on $L_y = 8$ and $L_y = 10$ cylinders, where solid lines denote the power-law fitting $D_A(r) \sim r^{-K_A}$ using the envelope of the data points (filled symbols). (c) Scalar chiral-chiral correlation $C(r)$ on $L_y = 10$ cylinders. Inset: Finite-size scaling of $C(L_x/4)$ on $L_y = 6, 8, 10$ cylinders as a function of $1/L_x$ using the second-order polynomial function. (d) Finite-size scaling of $C(L_x/4)$ as a function of $1/L_y$ on lattices with fixed ratio $L_x/L_y = 3$ using the second-order polynomial function.

showing a central charge $c \sim 1$ are also obtained by using the alternative approach in Ref. [49]. It is worth noting that in the limit $L_x = \infty$, our results show that $c \sim 1$ on all $L_y = 6$–12 cylinders (see Supplemental Material [46] for details) without notable dependence on L_y, suggesting that there is one gapless mode in the bulk of the system in two dimensions. It is hence reasonable to expect that the single gapless mode may carry momentum $k_2 = 0$ which is shared by all cylinders. To support this, we have further calculated $S(x)$, e.g., on an $N = 48 \times 8$ cylinder, by inserting a π flux through the cylinder where the momentum $k_2 = 0$ is unavailable. As expected, we find that $c \sim 0.1$ [see Fig. 3(d)], which is consistent with the absence of gapless mode.

We have also calculated the spin-spin correlation $F(r)$ as shown in Fig. 4(a) for $L_y = 6, 8, 10$ cylinders. For all cases, we find that $F(r)$ is short ranged and decays exponentially at long distances as $F(r) \sim e^{-r/\xi_s}$. Similar to the J_1-J_2 model, the correlation length is finite $\xi_s = 1.5$–3 as shown in the inset of Fig. 4(a). We have also calculated the spin triplet gap $\Delta = E_0(S_{tot} = 1) - E_0(S_{tot} = 0)$ on $L_y = 8$ cylinders [50], where $E_0(S_{tot})$ is the ground-state energy of the system with total spin S_{tot}. Our results show that Δ is finite in the bulk, which is consistent with short-range spin-spin correlation (see Supplemental Material [46] for more details). Contrary to the spin-spin correlation, we find that the dimer-dimer correlation decays as a power law at long distances as $D_a(r) \sim r^{-K_a}$ with a finite exponent K_a. In Fig. 4(b), we show that the exponent changes from $K_a \sim 1.8$ to $K_a \sim 1.2$ when the width

of the cylinder increases from $L_y = 8$ to $L_y = 10$. It is hence reasonable to conclude that the quasi-long-range dimer-dimer correlation is responsible for the single gapless mode.

To test the possibility of TRS breaking, we have measured the scalar chiral-chiral correlation function defined as

$$C(r) = \langle \hat{\chi}_{i_0} \hat{\chi}_{i_0+r} \rangle. \tag{5}$$

Here, $\hat{\chi}_i = \mathbf{S}_i \cdot (\mathbf{S}_j \times \mathbf{S}_k)$ is the scalar chiral operator defined on a small triangle, $i_0 = (x_0, y)$ is the reference point with $x_0 = L_x/4$, and r is the distance between two triangles in the $\mathbf{e}_1$ direction. Consistent with a previous study [28], we find that $C(r)$ remains finite on all cylinders and we even keep up to $m = 9000$ SU(2) states [equivalent to $m = 36\,000$ U(1) states]. Surprisingly, our results show that $C(r)$ decreases notably with the increase in L_x, which vanishes in the long-cylinder limit $L_x = \infty$ on all $L_y = 6, 8, 10$ cylinders after the finite-size scaling as shown in Fig. 4(c). To test the possibility of TRS breaking in two dimensions, we have also performed the finite-size scaling of $C(r)$ as a function of $1/L_y$ by fixing the lattice ratio $L_x/L_y = 3$. As an example, shown in Fig. 4(d), we find that $C(L_x/4)$ decreases rapidly with the increase in L_y and vanishes when L_y is large enough. This indicates a possibly vanishing chiral order in the two-dimensional limit. Therefore our results are consistent with the absence of long-range spin scalar chiral order, and the QSL phase of the J_1-J_2-J_3 model preserves the TRS.

Our results suggest that the ground state of the J_1-J_2-J_3 model is consistent with a critical spin liquid with a single gapless mode. To rule out the possibility that such critical behavior could be special to the point of $J_2 = 0.3$ and $J_3 = 0.15$, we have further considered a relatively distant parameter point in the J_1-J_2-J_3 spin liquid phase with $J_2 = 0.36$ and $J_3 = 0.24$ [28]. Following the same procedure, we have observed similar critical behavior with one gapless mode at this new point; detailed results are provided in the Supplemental Material [46]. Therefore our results suggest that the J_1-J_2-J_3 spin liquid is a critical phase [40] instead of a critical point.

Summary and discussion. We have studied the ground-state properties of the spin liquid phases in both the spin-1/2 J_1-J_2 and spin-1/2 J_1-J_2-J_3 models on the triangular lattice. Using large-scale parallel DMRG encoded with SU(2) spin rotational symmetry, we are able to obtain accurate results on notably longer systems by keeping a significantly large number of states in the DMRG simulation. Our results suggest that the QSL phase of the J_1-J_2 Heisenberg model is consistent with a gapped spin liquid which is characterized by the absence of a gapless spin mode and by short-range spin-spin and dimer-dimer correlations. In the presence of finite J_3 interaction, a critical spin liquid phase emerges which has one gapless mode and a quasi-long-range dimer-dimer correlation but an exponentially decaying spin-spin correlation.

A striking behavior of the central charge that is prominent on cylinder geometry is that its value can be notably affected by both the boundary and finite-size effects. While long cylinders are always necessary, we find that the reduced boundary effect brought about by removing a few data points close to the open ends of the cylinders can provide more reliable results that are much closer to those in the long-cylinder limit. However, it should be noted that some of the small-system behaviors presented here, including both the central charge and

[1] L. Balents, Nature (London) **464**, 199 (2010).

[2] L. Savary and L. Balents, Rep. Prog. Phys. **80**, 016502 (2017).

[3] C. Broholm, R. J. Cava, S. A. Kivelson, D. G. Nocera, M. R. Norman, and T. Senthil, Science **367**, eaay0668 (2020).

[4] P. W. Anderson, Science **235**, 1196 (1987).

[5] V. J. Emery, Phys. Rev. Lett. **58**, 2794 (1987).

[6] P. A. Lee, N. Nagaosa, and X. G. Wen, Rev. Mod. Phys. **78**, 17 (2006).

[7] C. Nayak, S. H. Simon, A. Stern, M. Freedman, and S. Das Sarma, Rev. Mod. Phys. **80**, 1083 (2008).

[8] E. Fradkin, S. A. Kivelson, and J. M. Tranquada, Rev. Mod. Phys. **87**, 457 (2015).

[9] T. Jolicoeur, E. Dagotto, E. Gagliano, and S. Bacci, Phys. Rev. B **42**, 4800 (1990).

[10] L. O. Manuel and H. A. Ceccatto, Phys. Rev. B **60**, 9489 (1999).

[11] R. V. Mishmash, J. R. Garrison, S. Bieri, and C. Xu, Phys. Rev. Lett. **111**, 157203 (2013).

[12] Y. Iqbal, W. J. Hu, R. Thomale, D. Poilblanc, and F. Becca, Phys. Rev. B **93**, 144411 (2016).

[13] Z. Zhu and S. R. White, Phys. Rev. B **92**, 041105(R) (2015).

[14] S. N. Saadatmand and I. P. McCulloch, Phys. Rev. B **94**, 121111(R) (2016).

[15] W. J. Hu, S. S. Gong, W. Zhu, and D. N. Sheng, Phys. Rev. B **92**, 140403(R) (2015).

[16] A. O. Scheie, E. A. Ghioldi, J. Xing, J. A. M. Paddison, N. E. Sherman, M. Dupont, D. Abernathy, D. M. Pajerowski, S.-S. Zhang, L. O. Manuel, A. E. Trumper, C. D. Pemmaraju, A. S. Sefat, D. S. Parker, T. P. Devereaux, J. E. Moore, C. D. Batista, and D. A. Tennant, arXiv:2109.11527.

[17] D. Kiese, Y. He, C. Hickey, A. Rubio, and D. M. Kennes, APL Mater. **10**, 031113 (2022).

[18] E. A. Ghioldi, S.-S. Zhang, Y. Kamiya, L. O. Manuel, A. E. Trumper, and C. D. Batista, Phys. Rev. B **106**, 064418 (2022).

[19] R. Kaneko, S. Morita, and M. Imada, J. Phys. Soc. Jpn. **83**, 093707 (2014).

[20] S. Hu, W. Zhu, S. Eggert, and Y.-C. He, Phys. Rev. Lett. **123**, 207203 (2019).

[21] P. H. Y. Li, R. F. Bishop, and C. E. Campbell, Phys. Rev. B **91**, 014426 (2015).

[22] W. Zheng, J.-W. Mei, and Y. Qi, arXiv:1505.05351.

[23] W.-J. Hu, S. S. Gong, and D. N. Sheng, Phys. Rev. B **94**, 075131 (2016).

[24] S. S. Gong, W. Zhu, J. X. Zhu, D. N. Sheng, and K. Yang, Phys. Rev. B **96**, 075116 (2017).

[25] D.-V. Bauer and J. O. Fjærestad, Phys. Rev. B **96**, 165141 (2017).

[26] A. Wietek and A. M. Läuchli, Phys. Rev. B **95**, 035141 (2017).

[27] F. Ferrari and F. Becca, Phys. Rev. X **9**, 031026 (2019).

[28] S. S. Gong, W. Zheng, M. Lee, Y.-M. Lu, and D. N. Sheng, Phys. Rev. B **100**, 241111(R) (2019).

[29] H. Kadowaki, H. Kikuchi, and Y. Ajiro, J. Phys.: Condens. Matter **2**, 4485 (1990).

[30] T. Kimura, J. C. Lashley, and A. P. Ramirez, Phys. Rev. B **73**, 220401(R) (2006).

[31] F. Ye, J. A. Fernandez-Baca, R. S. Fishman, Y. Ren, H. J. Kang, Y. Qiu, and T. Kimura, Phys. Rev. Lett. **99**, 157201 (2007).

[32] S. Seki, Y. Onose, and Y. Tokura, Phys. Rev. Lett. **101**, 067204 (2008).

[33] V. Kalmeyer and R. B. Laughlin, Phys. Rev. Lett. **59**, 2095 (1987).

[34] S. R. White, Phys. Rev. Lett. **69**, 2863 (1992).

[35] I. P. McCulloch and M. Gulácsi, Europhys. Lett. **57**, 852 (2002).

[36] G. K. Chan, J. Chem. Phys. **120**, 3172 (2004).

[37] R. Moessner and S. L. Sondhi, Phys. Rev. Lett. **86**, 1881 (2001).

[38] H. Yao and S. A. Kivelson, Phys. Rev. Lett. **108**, 247206 (2012).

[39] D. S. Rokhsar and S. A. Kivelson, Phys. Rev. Lett. **61**, 2376 (1988).

[40] H. Yao and D.-H. Lee, Phys. Rev. Lett. **107**, 087205 (2011).

[41] E. M. Stoudenmire and S. R. White, Phys. Rev. B **87**, 155137 (2013).

[42] J. Rincón, D. García, and K. Hallberg, Comput. Phys. Commun. **181**, 1346 (2010).

[43] S. Yamada, M. Okumura, T. Imamura, and M. Machida, Jpn. J. Ind. Appl. Math. **28**, 141 (2011).

[44] A. Kantian, M. Dolfi, M. Troyer, and T. Giamarchi, Phys. Rev. B **100**, 075138 (2019).

[45] R. Levy, E. Solomonik, and B. K. Clark, in *SC20: International Conference for High Performance Computing, Networking, Storage and Analysis* (IEEE, Piscataway, NJ, 2020), pp. 1–14.

[46] See Supplemental Material at http://link.aps.org/supplemental/10.1103/PhysRevB.107.L140411 for more details of the parallel DMRG, the benchmark results, an alternative way to extract the central charge, the spin gap of the two QSL phases, more results of the J_1-J_2-J_3 model, and preliminary results on wider systems.

[47] P. Calabrese and J. Cardy, J. Stat. Mech. (2004) P06002.

[48] M. Fagotti and P. Calabrese, J. Stat. Mech. (2011) P01017.

[49] S. Nishimoto, Phys. Rev. B **84**, 195108 (2011).

[50] S. Yan, D. A. Huse, and S. R. White, Science **332**, 1173 (2011).

[51] Y.-F. Jiang and H.-C. Jiang, Phys. Rev. Lett. **125**, 157002 (2020).

[52] C. Peng, Y.-F. Jiang, T. P. Devereaux, and H.-C. Jiang, npj Quantum Mater. **6**, 64 (2021).

[53] H.-C. Jiang, npj Quantum Mater. **6**, 71 (2021).